PHYSICAL REVIEW A VOLUME 44, NUMBER 3 1 AUGUST 1991

Autoionization and radiationless electron capture in complex spectra

J. Oreg,* W. H. Goldstein, and M. Klapisch
Lawrence Livermore National Laboratory, Livermore, California 94550

A. Bar-Shalom*
Department of Physics and Space Science Laboratory, University of California, Berkeley, Berkeley, California 94720
(Received 5 December 1990)

The factorization-interpolation model, developed to compute collisional excitation rate coefficients efficiently in dense plasma, is applied here to autoionization and radiationless electron capture. Results using a parametric atomic central potential and factorization interpolation for autoionization rates and dielectronic recombination rate coefficients in Ne-like Fe are compared to multiconfigurational Dirac-Fock calculations. Agreement is very good. As a further application, we treat the problem of indirect ionization via collisional excitation followed by autoionization in Zn-like Mo.

I. INTRODUCTION

Successful modeling of plasma spectra taken in a variety of current experiments, including x-ray laser, plasma fusion, and astrophysical work, depends heavily on computing accurate cross sections for the processes populating the atomic levels in the plasma. For this purpose, several relativistic distorted-wave programs were developed and used extensively in the past decade [1]. Still, the vast number of detailed, relativistic, quantum-mechanical calculations needed to model the kinetics in dense plasmas required new techniques to speed up computations.

Recently, the factorization-interpolation (FI) method [2] was introduced for calculating a large array of relativistic distorted-wave collisional excitation cross sections from a relatively small set of radial integrals. Since radial integrals are the bottleneck in these problems, the method significantly improved computational efficiency. Factorization interpolation of collisional excitation cross sections has already been extensively used by several groups [3–5], combined either with the relativistic-parametric-potential model [6], or with the Dirac-Fock-Slater method [4].

In this work, we extend the FI method to autoionization and electron capture between systems with $N+1$ and N bound electrons. Computer codes based on the multiconfigurational Dirac-Fock (MCDF) model and the distorted-wave approximation are already available for calculating rates for these processes [1, 7]. In addition to using the FI method, the present work improves on existing models in adopting the relativistic, multiconfigurational, parametric potential (RPP) for determining atomic wave functions, energies, and transition probabilities. In the RPP model, a single, analytic, variationally determined potential is used for both bound and continuum orbitals, and for both initial and final configurations. In general, RPP reproduces Dirac-Fock calculations, while exceeding them in speed and stability, and avoiding nonorthogonal orbitals. The RPP model is the basis of the atomic structure code RELAC [3], used widely in highly charged, heavy-ion spectroscopy. Furthermore, the RPP, together with the FI method, underlies the HULLAC package of collisional-radiative modeling codes, which now generate autoionization rates in addition to atomic structure, radiative transitions, and collisional excitation rates, using a consistent set of wavefunctions for all processes.

Our FI-RPP calculations are tested here by comparison to MCDF results. As an application of the model we treat the problem of excitation autoionization, which has been found to significantly enhance ionization rates in recent tokamak experiments [8–10]. The method presented here has already been applied to resonant excitation in Ne-like Fe [11].

II. AUTOIONIZATION IN THE FI-RPP MODEL

The RPP method [3] was developed originally for calculating bound-bound relativistic transition energies and intensities. The main idea of this approach is the introduction of a central potential as an analytic function of screening parameters which are determined by minimizing the first-order relativistic energy of a set of levels or configurations. This optimized potential is used to caiculate all one-electron orbitals and energies, relativistic multiconfiguration bound states and their energies, and all the required radiative transition rates. For collisional excitation, the same potential, with a slight correction at large-r values, is used also for calculating the continuum orbitals. The potential acting upon the continuum electron far from the ion is screened by an additional electron compared to the potential acting upon a bound electron of that ion. For the calculation of the continuum orbital therefore we use the bound potential corrected smoothly at large r for this difference. Since the bound orbital vanishes at these large-r values, the continuum and bound orbitals remain orthogonal. For autoionization when using the autoionizing configuration potential this correction procedure is not required.

It was shown in Ref. [2] that the collisional excitation strength can be factorized in the following way:

$$\Omega_{01}=8\sum_{t}\sum_{\mathbf{j}_0,\mathbf{j}_1}\sum_{\mathbf{j}'_0,\mathbf{j}'_1}\langle\psi_0\|\mathbf{Z}^{(t)}(\mathbf{j}_0,\mathbf{j}_1)\|\psi_1\rangle\langle\psi_0\|\mathbf{Z}^{(t)}(\mathbf{j}'_0,\mathbf{j}'_1)\|\psi_1\rangle Q^t(\mathbf{j}_0,\mathbf{j}_1;\mathbf{j}'_0,\mathbf{j}'_1)\ , \tag{1}$$

where

$$\mathbf{Z}^{(t)}(\mathbf{j}_0,\mathbf{j}_1)=\sum_i \mathbf{Z}_i^{(t)}(\mathbf{j}_0,\mathbf{j}_1) \tag{2}$$

is the multipole unit operator defined by the reduced matrix element

$$\langle\mathbf{j}_a\|\mathbf{Z}^{(t)}(\mathbf{j},\mathbf{j}')\|\mathbf{j}_b\rangle\equiv\delta_{\mathbf{j}\mathbf{j}_a}\delta_{\mathbf{j}'\mathbf{j}_b}\ . \tag{3}$$

In Eq. (1) ψ_0 and ψ_1 are the generally mixed configuration initial and final levels of the transition and $\mathbf{j}_0,\mathbf{j}_1$ and $\mathbf{j}'_0,\mathbf{j}'_1$ represent the quantum numbers nlj of the one-electron orbitals involved. The factorized radial factor Q^k includes the sum over continuum partial waves and contains both the direct and exchange contributions to the cross section. It is defined and discussed in detail in Ref. [2]. We only point out here that it was shown to be a slowly varying function of the transition energy and needs therefore to be calculated only for a few energy points which serve to interpolate the whole transition array.

The dielectronic capture rate from an initial target state ψ to all states in the autoionizing level ψ'' of the neighboring charge state is [12]

$$D_{\psi}^{\psi''}=(1/g)f\sum_{M_T''}A_{\psi}^{\psi''}\ , \tag{4}$$

where

$$f=f(\Delta E_{\psi\psi''})=N_e\tfrac{1}{2}(h^2/2\pi m_e kT_e)^{3/2}\exp(-\Delta E_{\psi\psi'}/kT_e)$$

is obtained from detailed balance and the electron distribution function at temperature T_e and density N_e, and g is the statistical weight of ψ, $g\equiv[J]\equiv 2J+1$.

$A_{\psi}^{\psi''}$ is the autoionization rate from state ψ'' to ψ:

$$A_{\psi}^{\psi''}=\sum_{\tilde{\mathbf{j}}}\sum_{J_T,M_T}\left|\left\langle\psi(\Gamma,J)\tilde{\mathbf{j}}J_TM_T\left|\sum_{\substack{i,j\\ i<j}}\left[\frac{e}{r_{ij}}\right]\right|\psi''(\Gamma'',J_T'',M_T'')\right\rangle\right|^2\ . \tag{5}$$

The outer sum here is over continuum orbitals $\tilde{\mathbf{j}}\equiv(E_{\tilde{\mathbf{j}}},l_{\tilde{\mathbf{j}}},\hat{j})$. Note that by conservation of angular momentum only one term contributes to the sum over J_T,M_T in Eq. (5).

It is desired to use the same potential for all the transitions of the two charge states involved in Eq. (5). This approximation yields a set of orthogonal states for the whole model, and bypasses the complexity of overlapping nonactive orbitals. As shown later on, an acceptable potential is the one obtained by minimizing the energies of the autoionizing states.

The use of an orthogonal set for all bound and continuum orbitals allows the separation of the continuum from Eq. (5) yielding (see Appendixes A and B)

$$A_{\psi}^{\psi''}=\sum_{\tilde{\mathbf{j}}}\left[\sum_{t}\sum_{\mathbf{j}_0,\mathbf{j}_a,\mathbf{j}_b}(-1)^{J-J_T''+j_b}\langle\psi\|[\mathbf{Z}^{(t)}(\mathbf{j}_0,\mathbf{j}_a)\times\mathbf{a}_{\mathbf{j}_b}]^{(\tilde{j})}\|\psi''\rangle\phi^t(\mathbf{j}_0\tilde{\mathbf{j}},\mathbf{j}_a\mathbf{j}_b)\right]^2\ , \tag{6}$$

where $\mathbf{a}_{\mathbf{j}_b}$ is the annihilation tensor operator, $\mathbf{j}_a\mathbf{j}_b$ are the doubly excited orbitals in ψ'', and $\mathbf{j}_0$ is the orbital which makes the internal transition in ψ. The bound states are decoupled from the continuum and the angular matrix element involves only the bound states. However, the matrix element is not completely factorized from the continuum because of the rank $\tilde{j}$ in the operator. For collisional excitation [Eq. (1)], infinite continuum partial waves $\tilde{\mathbf{j}},\tilde{\mathbf{j}}'$ exist and convergence must be reached. In this case the complete factorization played an important role. On the other hand, in Eq. (6) the continuum partial waves $\tilde{\mathbf{j}}$ are restricted by triangle conditions involving only bound orbitals $(\mathbf{j}_0\mathbf{j}_a\mathbf{j}_b)$. Thus the factorization of Eq. (6) is not essential to the interpolation but can enhance computational speed. As for collisional excitation, each radial integral $\phi^t(\mathbf{j}_0\tilde{\mathbf{j}},\mathbf{j}_a\mathbf{j}_b)$, appears many times for many transitions. In principle this integral depends on each transition ψ-ψ'' due to the conservation of energy of the bound plus continuum system. Fortunately, as in

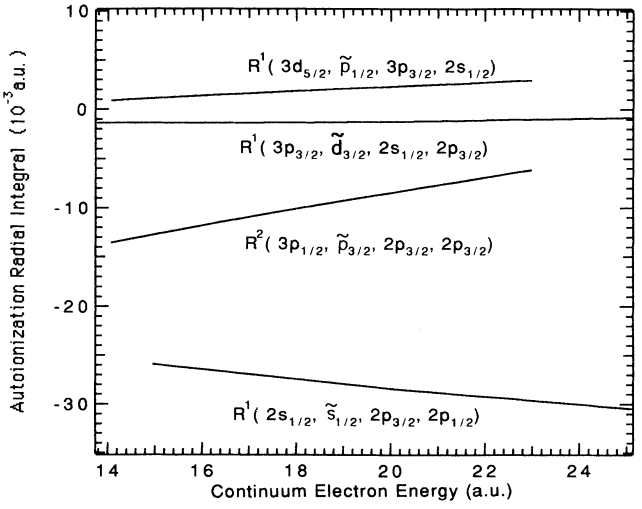

FIG. 1. Energy dependence of autoionization radial Slater integrals (the tilde denotes the continuum orbital).

the collisional excitation case, we have found that this dependence is weak enough so that with a few energy points one can interpolate the whole transition array without loss of accuracy. The weak dependence of the autoionization radial integrals on the transition energy was noticed in all of our many observations. A typical behavior of autoionization Slater integrals versus transition energy is demonstrated in Fig. 1. As in the case of collisional excitation, the use of interpolation reduces the computation time drastically. For example, for the rela-

TABLE I. Comparison between the FI-RPP and the MCDF results for autoionization rates (in 10^{12} sec^{-1}) of selenium Ne-like doubly excited states into the two states $2p^5_{1/2}$ and $2p^5_{3/2}$ of the F-like ions. The levels are designated by their large zero-order component. (Brakets denote the coupling scheme, e.g., $[(j_1,j_2)_a j_3]_b$ means that j_1 and j_2 are coupled to a with a and j_3 coupled to b.)

Final F-like level	Initial Ne-like autoionizing level	J	$2p^2_{1/2}2p^3_{3/2}$ FI-RPP	$2p^2_{1/2}2p^3_{3/2}$ MCDF	$2p_{1/2}2p^4_{3/2}$ FI-RPP	$2p_{1/2}2p^4_{3/2}$ MCDF
1	$(2p^2_{1/2}2p^2_{3/2})_0 3s^2$	0	0.85	0.75	13.3	12.0
2	$2p^4_{3/2}3s^2$	0	13.0	11.5	0.84	0.77
3	$(2p_{1/2}2p^3_{3/2})_1 3s^2$	1	7.11	6.41	6.96	6.14
4	$(2p^2_{1/2}2p^2_{3/2})_2 3s^2$	2	0.17	0.15	14.0	12.6
5	$(2p_{1/2}2p^3_{3/2})_2 3s^2$	2	6.93	6.24	7.11	6.31
6	$[(2p^2_{1/2}2p^2_{3/2})_0 3s]_{1/2}3p_{1/2}$	0	0.003	0.001	0.21	0.18
7	$[(2p_{1/2}2p^3_{3/2})_1 3s]_{1/2}3p_{1/2}$	0	0.000 009	0.0003	0.32	0.27
8	$[(2p^4_{3/2}3s)_{1/2}3p_{1/2}$	0	168	142	0.03	0.03
9	$[(2p^2_{1/2}2p^2_{3/2})_2 3s]_{3/2}3p_{3/2}$	0	0.78	0.74	0.73	0.58
10	$[(2p_{1/2}2p^3_{3/2})_1 3s]_{3/2}3p_{3/2}$	0	5.69	4.87	0.21	0.17
11	$[(2p_{1/2}2p^3_{3/2})_2 3s]_{3/2}3p_{3/2}$	0	188	175	0.003	0.001
12	$[(2p^2_{1/2}2p^2_{3/2})_0 3s]_{1/2}3p_{1/2}$	1	0.002	0.003	0.84	0.84
13	$[(2p^2_{1/2}2p^2_{3/2})_2 3s]_{3/2}3p_{1/2}$	1	0.13	0.12	0.50	0.42
14	$[(2p_{1/2}2p^3_{3/2})_2 3s]_{1/2}3p_{1/2}$	1	0.41	0.34	11.6	11.0
15	$[(2p_{1/2}2p^3_{3/2})_1 3s]_{3/2}3p_{1/2}$	1	0.78	0.60	10.5	11.9
16	$[(2p_{1/2}2p^3_{3/2})_2 3s]_{3/2}3p_{1/2}$	1	34.9	31.5	154	124
17	$[(2p^4_{3/2})_0 3s]_{1/2}3p_{1/2}$	1	152	131	3.21	2.66
18	$[(2p^2_{1/2}2p^2_{3/2})_0 3s]_{1/2}3p_{3/2}$	1	1.57	1.44	20.4	19.6
19	$[(2p^2_{1/2}2p^2_{3/2})_2 3s]_{3/2}3p_{3/2}$	1	0.34	0.33	1.25	1.32
20	$[(2p^2_{1/2}2p^2_{3/2})_2 3s]_{5/2}3p_{3/2}$	1	1.20	1.22	54.2	54.9
21	$[(2p_{1/2}3p^3_{3/2})_1 3s]_{1/2}3p_{3/2}$	1	1.71	1.75	6.90	6.12
22	$[(2p_{1/2}3p^3_{3/2})_1 3s]_{3/2}3p_{3/2}$	1	0.89	1.10	80.6	75.9
23	$[(2p_{1/2}2p^3_{3/2})_2 3s]_{3/2}3p_{3/2}$	1	0.15	0.16	8.57	6.63
24	$[(2p_{1/2}2p^3_{3/2})_2 3s]_{5/2}3p_{3/2}$	1	143	133	84.3	74.7
25	$[(2p^4_{3/2})_0 3s]_{1/2}3p_{3/2}$	1	64.3	54.9	3.02	2.60
26	$[(2p^2_{1/2}2p^2_{3/2})_2 3s]_{3/2}3p_{1/2}$	2	0.007	0.006	1.15	0.93
27	$[(2p^2_{1/2}2p^2_{3/2})_2 3s]_{5/2}3p_{1/2}$	2	0.002	0.001	0.19	0.16
28	$[(2p_{1/2}2p^3_{3/2})_1 3s]_{3/2}3p_{1/2}$	2	0.11	0.097	13.6	12.7
29	$[(2p_{1/2}2p^3_{3/2})_2 3s]_{3/2}3p_{1/2}$	2	0.90	0.73	2.29	2.23
30	$[(2p_{1/2}2p^3_{3/2})_2 3s]_{5/2}3p_{1/2}$	2	0.009	0.008	39.9	29.7
31	$[(2p^2_{1/2}2p^2_{3/2})_0 3s]_{1/2}3p_{3/2}$	2	0.004	0.004	1.17	1.11
32	$[(2p^2_{1/2}3p^2_{3/2})_2 3s]_{3/2}3p_{3/2}$	2	0.002	0.001	8.45	8.40
33	$[(2p^2_{1/2}2p^2_{3/2})_2 3s]_{5/2}3p_{3/2}$	2	0.02	0.02	62.6	59.1
34	$[(2p_{1/2}2p^3_{3/2})_1 3s]_{1/2}3p_{3/2}$	2	0.40	0.35	44.0	53.1
35	$[(2p_{1/2}2p^3_{3/2})_1 3s]_{3/2}3p_{3/2}$	2	0.44	0.35	1.43	1.35
36	$[(2p_{1/2}2p^3_{3/2})_2 3s]_{3/2}3p_{3/2}$	2	0.03	0.04	151	123
37	$[(2p_{1/2}2p^3_{3/2})_2 3s]_{5/2}3p_{1/2}$	2	0.09	0.04	39.2	32.7
38	$[(2p^4_{3/2})_0 3s]_{1/2}3p_{3/2}$	2	0.97	0.78	0.92	0.81
39	$[(2p^2_{1/2}2p^2_{3/2})_2 3s]_{5/2}3p_{1/2}$	3	0.000 9	0.000 7	0.24	0.19
40	$[(2p_{1/2}2p^3_{3/2})_2 3s]_{5/2}3p_{1/2}$	3	0.31	0.24	0.32	0.27
41	$[(2p^2_{1/2}2p^2_{3/2})_2 3s]_{3/2}3p_{3/2}$	3	0.001	0.001	0.30	0.26
42	$[(2p^2_{1/2}2p^2_{3/2})_2 3s]_{5/2}3p_{3/2}$	3	0.005	0.004	0.52	0.40
43	$[(2p_{1/2}2p^3_{3/2})_1 3s]_{3/2}3p_{3/2}$	3	0.026	0.022	0.37	0.29
44	$[(2p_{1/2}2p^3_{3/2})_2 3s]_{3/2}3p_{3/2}$	3	0.19	0.17	0.19	0.16
45	$[(2p_{1/2}2p^3_{3/2})_2 3s]_{5/2}3p_{3/2}$	3	0.42	0.34	0.50	0.40
46	$[(2p^2_{1/2}2p^2_{3/2})_2 3s]_{5/2}3p_{3/2}$	4			0.15	0.12
47	$[(2p_{1/2}2p^3_{3/2})_2 3s]_{5/2}3p_{3/2}$	4			0.92	0.74

tively simple case of Ne-like to F-like autoionization, only about 1% of the integrals needed to be calculated.

In order to establish the accuracy of our method we compare in the next section our results with the MCDF method [7, 13].

III. COMPARISON WITH THE MCDF RESULTS

A. Autoionization rates for Ne-F like Se

In Table I we present the autoionization rates from the doubly excited states of the Ne-like configurations,

$$(2p^2_{1/2}2p^2_{3/2}3s^2+2p_{1/2}2p^3_{3/2}3s^2+2p^4_{3/2}3s^2)+(2p^2_{1/2}2p^2_{3/2}3s3p_{1/2}+2p_{1/2}2p^3_{3/2}3s3p_{1/2}+2p^4_{3/2}3s3p_{1/2})$$
$$+(2p^2_{1/2}2p^2_{3/2}3s3p_{3/2}+2p^1_{1/2}2p^3_{3/2}3s3p_{3/2}+2p^4_{3/2}3s3p_{3/2}),$$

to the two F-like states $2p^5_{1/2}$ and $2p^5_{3/2}$ in Se.

The rates were calculated in both the FI-RPP model and the MCDF model [13]. In most cases the agreement is better than 10% and except for small rates that are very sensitive to configuration mixing (some are nonzero owing only to a small mixing component), it is always within 20%. It should be noticed also that the deviations are systematic. Generally the FI-RPP results are higher than those of the MCDF.

We expect that the "best" potential should be that which minimizes energies of the doubly excited states, since the neighboring ion's ground state lie in the same energy range. We found, however, that our results are not greatly sensitive to the choice of potential. Using potentials obtained by minimizing the doubly excited states, the singly excited states or the ground states of both ions yielded difference of no more than 25% in the autoionization rates.

B. Dielectronic recombination rates for F-like iron

In this example we present results for dielectronic recombination (DR) rates for F-like iron at an electron temperature of $T_e = 1000$ eV.

In the isolated resonance approximation, the rate for the two-step capture, radiative decay process, from ψ_0 to ψ_1, is given by [12]

$$\mathcal{R}_{01}=\sum_{\psi''}\left[D^{\psi''}_{\psi_0}A^{\psi''}_{\psi_1}\Big/\sum_{\psi'}(A^{\psi''}_{\psi'}+R^{\psi''}_{\psi'})\right], \tag{7}$$

where $\sum_{\psi'} R^{\psi''}_{\psi'}$ is the radiative decay rate from ψ'' to all states ψ' in the model. The DR rates from the F-like configurations, $2p^5, 2s2p^6$ to the 37 relativistic levels of the Ne-like configurations $(2p^6+2p^53s+2p^53p+2p^53d)$ at $T_e = 1$ keV are given in Tables II and III. All the doubly excited states ψ'' of the configuration $2p^43131'$ are included. Again we present for comparison the (MCDF) results [13] as well. The agreement is very good (better than 5%). This level of agreement is not surprising since the sum in Eq. (7) is dominated by the largest autoionization rates.

IV. EXCITATION-AUTOIONIZATION IN Zn-LIKE MO

Spectral analysis of tokamak plasmas has recently shown evidence of the very significant contribution of excitation-autoionization processes to the ionization equi-

TABLE II. Identification of Ne-like and F-like mixed configuration levels, by their largest zero-order component.

	Ne-like even levels	$2j+1$
1	$2s^22p^2_{1/2}2p^3_{3/2}3p_{1/2}$	3
2	$2s^22p^2_{1/2}2p^3_{3/2}3p_{1/2}$	5
3	$2s^22p^2_{1/2}2p^3_{3/2}3p_{1/2}$	7
4	$2s^22p^2_{1/2}2p^3_{3/2}3p_{3/2}$	3
5	$2s^22p^2_{1/2}2p^3_{3/2}3p_{3/2}$	5
6	$2s^22p^2_{1/2}2p^3_{3/2}3p_{3/2}$	1
7	$2s^22p_{1/2}2p^4_{3/2}3p_{1/2}$	3
8	$2s^22p_{1/2}2p^4_{3/2}3p_{3/2}$	3
9	$2s^22p_{1/2}2p^4_{3/2}3p_{3/2}$	5
10	$2s^22p_{1/2}2p^4_{3/2}3p_{1/2}$	1
11	$2s2p^2_{1/2}2p^4_{3/2}3s$	3
12	$2s2p^2_{1/2}2p^4_{3/2}3s$	1
13	$2s2p^2_{1/2}2p^4_{3/2}3d_{1/2}$	3
14	$2s2p^2_{1/2}2p^4_{3/2}3d_{1/2}$	5
15	$2s2p^2_{1/2}2p^4_{3/2}3d_{3/2}$	7
16	$2s2p^2_{1/2}2p^4_{3/2}3d_{3/2}$	5
	Ne-like odd levels	$2j+1$
1	$2s^22p^2_{1/2}2p^3_{3/2}3s$	1
2	$2s^22p^2_{1/2}2p^3_{3/2}3s$	3
3	$2s^22p_{1/2}2p^4_{3/2}3s$	1
4	$2s^22p_{1/2}2p^4_{3/2}3s$	3
5	$2s^22p^2_{1/2}2p^3_{3/2}3d_{3/2}$	1
6	$2s^22p^2_{1/2}2p^3_{3/2}3d_{1/2}$	3
7	$2s^22p^2_{1/2}2p^3_{3/2}3d_{3/2}$	5
8	$2s^22p^2_{1/2}2p^3_{3/2}3d_{3/2}$	9
9	$2s^22p^2_{1/2}2p^3_{3/2}3d_{1/2}$	7
10	$2s^22p^2_{1/2}2p^3_{3/2}3d_{1/2}$	5
11	$2s^22p^2_{1/2}2p^3_{3/2}3d_{3/2}$	7
12	$2s^22p^2_{1/2}2p^3_{3/2}3d_{3/2}$	3
13	$2s^22p_{1/2}2p^4_{3/2}3d_{1/2}$	5
14	$2s^22p_{1/2}2p^4_{3/2}3d_{3/2}$	5
15	$2s^22p_{1/2}2p^4_{3/2}3d_{3/2}$	7
16	$2s^22p_{1/2}2p^4_{3/2}3d_{1/2}$	3
17	$2s2p^2_{1/2}2p^4_{3/2}3p_{1/2}$	1
18	$2s2p^2_{1/2}2p^4_{3/2}3p_{1/2}$	3
19	$2s2p^2_{1/2}2p^4_{3/2}3p_{3/2}$	5
20	$2s2p^2_{1/2}2p^4_{3/2}3p_{3/2}$	3
	F-like levels	$2j+1$
1′	$2s^22p^2_{1/2}2p^3_{3/2}$	4
2′	$2s^22p_{1/2}2p^4_{3/2}$	2
3′	$2s2p^2_{1/2}2p^4_{3/2}$	2

TABLE III. Dielectronic recombination rates (in 10^{-12} sec^{-1} cm^3) for the even and odd configurations of F-like iron at $T=1$ keV. Comparison between results of the FI-RPP and the MCDF methods. 1′,2′,3′ designate the F-like initial levels. The levels are identified by their sequential number in Table II.

	Even							Odd					
	1′		2′		3′			1′		2′		3′	
	FI	MCDF	FI	MCDF	FI	MCDF		FI	MCDF	FI	MCDF	FI	MCDF
1	0.151	0.252	0.103	0.091	0.040	0.037	1	0.254	0.236	0.124	0.139	0.012	0.012
2	0.258	0.254	0.138	0.131	0.033	0.031	2	0.144	0.140	0.175	0.170	0.008	0.007
3	0.336	0.322	0.164	0.163	0.037	0.034	3	0.010	0.012	0.080	0.078	0.005	0.005
4	0.119	0.120	0.130	0.120	0.032	0.030	4	0.082	0.075	0.233	0.211	0.017	0.015
5	0.246	0.251	0.164	0.142	0.038	0.037	5	0.037	0.036	0.017	0.019	0.009	0.008
6	0.045	0.047	0.046	0.042	0.013	0.012	6	0.101	0.109	0.075	0.065	0.026	0.023
7	0.103	0.110	0.200	0.189	0.034	0.032	7	0.162	0.163	0.213	0.216	0.041	0.037
8	0.085	0.084	0.205	0.196	0.034	0.032	8	0.440	0.435	0.271	0.288	0.060	0.054
9	0.158	0.166	0.346	0.273	0.052	0.050	9	0.287	0.298	0.235	0.223	0.045	0.045
10	0.038	0.036	0.076	0.080	0.013	0.012	10	0.181	0.184	0.191	0.188	0.042	0.039
11	0.087	0.090	0.108	0.121	0.096	0.107	11	0.268	0.273	0.310	0.304	0.053	0.055
12	0.021	0.023	0.026	0.034	0.092	0.086	12	0.103	0.110	0.129	0.120	0.033	0.032
13	0.012	0.012	0.012	0.014	0.250	0.275	13	0.114	0.121	0.318	0.315	0.054	0.052
14	0.026	0.028	0.002	0.003	0.460	0.507	14	0.121	0.124	0.270	0.273	0.072	0.065
15	0.040	0.043	0.054	0.056	0.751	0.806	15	0.172	0.169	0.491	0.504	0.072	0.071
16	0.024	0.029	0.036	0.043	0.470	0.495	16	0.109	0.100	0.233	0.244	0.049	0.048
							17	0.006	0.006	0.004	0.004	0.092	0.073
							18	0.016	0.017	0.014	0.014	0.276	0.237
							19	0.030	0.029	0.027	0.033	0.485	0.460
							20	0.012	0.015	0.017	0.020	0.297	0.302

librium of high-Z elements [8–10]. As an application of our FI-RPP method we present in this section the calculation of indirect ionization rates for Zn-like Mo ions. These results are compared with direct impact ionization rates.

In the isolated resonance approximation, the indirect ionization rate $X(g,k)$ from the Zn-like $3d^{10}4s^2$ ground state (g) to level k of the Cu-like configurations is given by

$$X(g,k)=\sum_j Q_{gj}\,A_{jk}\Big/\sum_l (A_{jl}+R_{jl})\ , \tag{8}$$

where Q_{gj} is the collisional excitation rate from the state g to level j of a Zn I–like $3d^9 4s^2 4p, -4d, -4f$ configuration, and A_{jk}, R_{jl} are the autoionization and radiative decay rates from state j to levels k and l, respectively.

The list of levels involved in the model is given in Table IV in increasing energy order. For each indirect channel $g-j-k$ we list in Table V the rates of the processes involved for the electron temperatures range 100–350 eV (the ionization potential of Zn-like Mo is $\chi=275$ eV).

The total indirect ionizations are compared with direct ionization rate obtained as an estimate from the Lotz formula [14]. The results indicate clearly the dominance of the indirect channel over direct ionization and the need to take this indirect process into account for the determination of the ionization balance.

V. SUMMARY

In this work we have extended the FI-RPP model to include electronic capture and autoionization. It was shown that, like collisional excitation, the factorization interpolation technique reduces the required computer time drastically without loss of accuracy. We have presented results for autoionization rates in Ne-like Se and showed good agreement with the MCDF model. We then presented DR rates for F-like to Ne-like iron. These results are shown to agree to better than 5% with MCDF results. Finally we introduced detailed calculations for dielectronic recombination rates for F- to Ne-like iron, and indirect ionization in Zn I–like Mo tokamak ions.

ACKNOWLEDGMENT

We thank Dr. M. H. Chen for useful discussions and for MCDF data for comparison.

APPENDIX A: THE "DIRECT" REPRESENTATION OF THE ELECTROSTATIC INTERACTION

When the radial and angular dependences of the electrostatic operator are completely separated, it takes the form [15,16]

$$\sum_{\substack{i,j\\ i<j}} e/r_{ij}=\sum_{\mathrm{j}_a,\mathrm{j}_b,\mathrm{j}'_a,\mathrm{j}'_b}\ \sum_{\substack{i,j\\ i\neq j}} [\mathbf{Z}_i^{(t)}(\mathrm{j}_a,\mathrm{j}_{a'})\cdot\mathbf{Z}_j^{(t)}(\mathrm{j}_b,\mathrm{j}_{b'})]\phi^t(\mathrm{j}_a\mathrm{j}_b,\mathrm{j}_{a'}\mathrm{j}_{b'})\ . \tag{A1}$$

TABLE IV. Zn-like plus Cu-like Mo energy levels (Cu-like levels are underlined.)

	Level	$2J+1$	Energy (cm^{-1})		Level	$2J+1$	Energy (cm^{-1})
1	$3d^4_{3/2}3d^6_{5/2}4s^2$	1	0.0	29	$3d^3_{3/2}3d^6_{5/2}4s^24d_{5/2}$	5	2 271 537.7
2	$3d^4_{3/2}3d^5_{5/2}4s^24p_{1/2}$	5	1 795 873.2	30	$3d^3_{3/2}3d^6_{5/2}4s^24d_{3/2}$	5	2 273 740.9
3	$3d^4_{3/2}3d^5_{5/2}4s^24p_{1/2}$	7	1 802 107.0	31	$3d^3_{3/2}3d^6_{5/2}4s^24d_{5/2}$	7	2 275 551.3
4	$3d^3_{3/2}3d^6_{5/2}4s^24p_{1/2}$	5	1 823 994.7	32	$3d^4_{3/2}3d^5_{5/2}4s^24d_{5/2}$	1	2 438 033.1
5	$3d^4_{3/2}3d^5_{5/2}4s^24p_{3/2}$	3	1 824 896.5	33	$3d^4_{3/2}3d^6_{5/2}4p_{1/2}$	2	2 467 560.2
6	$3d^4_{5/2}3d^5_{5/2}4s^24p_{3/2}$	9	1 827 783.5	34	$3d^4_{3/2}3d^6_{5/2}4p_{3/2}$	4	2 498 402.6
7	$3d^4_{3/2}3d^5_{5/2}4s^24p_{3/2}$	5	1 838 441.0	35	$3d^4_{3/2}3d^5_{5/2}4s^24f_{5/2}$	1	2 615 697.0
8	$3d^4_{3/2}3d^5_{5/2}4s^24p_{3/2}$	7	1 842 454.8	36	$3d^4_{3/2}3d^5_{5/2}4s^24f_{5/2}$	3	2 618 281.5
9	$3d^3_{3/2}3d^6_{5/2}4s^24p_{3/2}$	1	1 844 670.8	37	$3d^4_{3/2}3d^5_{5/2}4s^24f_{7/2}$	5	2 622 352.0
10	$3d^3_{3/2}3d^6_{5/2}4s^24p_{1/2}$	3	1 844 809.5	38	$3d^4_{3/2}3d^5_{5/2}4s^24f_{7/2}$	13	2 624 477.6
11	$3d^3_{3/2}3d^6_{5/2}4s^24p_{3/2}$	7	1 859 019.1	39	$3d^4_{3/2}3d^5_{5/2}4s^24f_{5/2}$	11	2 626 322.0
12	$3d^3_{3/2}3d^6_{5/2}4s^24p_{3/2}$	3	1 863 103.2	40	$3d^4_{3/2}3d^5_{5/2}4s^24f_{5/2}$	5	2 630 752.0
13	$3d^3_{3/2}3d^6_{5/2}4s^24p_{3/2}$	5	1 867 441.9	41	$3d^4_{3/2}3d^5_{5/2}4s^24f_{7/2}$	7	2 631 196.6
14	$3d^4_{3/2}3d^5_{5/2}4s^24d_{3/2}$	3	2 217 330.2	42	$3d^4_{3/2}3d^5_{5/2}4s^24f_{7/2}$	9	2 633 456.9
15	$3d^4_{3/2}3d^6_{5/2}4s$	2	2 231 383.8	43	$3d^4_{3/2}3d^5_{5/2}4s^24f_{5/2}$	9	2 634 690.1
16	$3d^4_{3/2}3d^5_{5/2}4s^24d_{3/2}$	9	2 233 600.0	44	$3d^4_{3/2}3d^5_{5/2}4s^24f_{7/2}$	11	2 635 296.9
17	$3d^4_{3/2}3d^5_{5/2}4s^24d_{5/2}$	11	2 235 474.2	45	$3d^4_{3/2}3d^5_{5/2}4s^24f_{5/2}$	7	2 637 166.6
18	$3d^4_{3/2}3d^5_{5/2}4s^24d_{3/2}$	5	2 235 557.1	46	$3d^4_{3/2}3d^5_{5/2}4s^24f_{7/2}$	3	2 640 210.0
19	$3d^4_{3/2}3d^5_{5/2}4s^24d_{5/2}$	3	2 236 539.8	47	$3d^3_{3/2}3d^6_{5/2}4s^24f_{7/2}$	5	2 649 771.9
20	$3d^4_{3/2}3d^5_{5/2}4s^24d_{3/2}$	7	2 240 945.9	48	$3d^3_{3/2}3d^6_{5/2}4s^24f_{5/2}$	9	2 653 430.9
21	$3d^4_{3/2}3d^5_{5/2}4s^24d_{5/2}$	7	2 245 309.3	49	$3d^3_{3/2}3d^6_{5/2}4s^24f_{7/2}$	11	2 654 798.1
22	$3d^4_{3/2}3d^5_{5/2}4s^24d_{5/2}$	5	2 248 241.4	50	$3d^3_{3/2}3d^6_{5/2}4s^24f_{5/2}$	5	2 657 862.9
23	$3d^4_{3/2}3d^5_{5/2}4s^24d_{5/2}$	9	2 249 021.9	51	$3d^3_{3/2}3d^6_{5/2}4s^24f_{7/2}$	7	2 659 766.3
24	$3d^3_{3/2}3d^6_{5/2}4s^24d_{3/2}$	1	2 249 523.6	52	$3d^3_{3/2}3d^6_{5/2}4s^24f_{7/2}$	9	2 662 562.8
25	$3d^3_{3/2}3d^6_{5/2}4s^24d_{5/2}$	3	2 256 468.6	53	$3d^3_{3/2}3d^6_{5/2}4s^24f_{5/2}$	7	2 664 125.8
26	$3d^3_{3/2}3d^6_{5/2}4s^24d_{3/2}$	7	2 260 127.2	54	$3d^3_{3/2}3d^6_{5/2}4s^24f_{5/2}$	3	2 697 935.0
27	$3d^3_{3/2}3d^6_{5/2}4s^24d_{3/2}$	3	2 263 512.3	55	$3d^4_{3/2}3d^6_{5/2}4d_{3/2}$	4	2 879 687.4
28	$3d^3_{3/2}3d^6_{5/2}4s^24d_{5/2}$	9	2 266 773.2	56	$3d^4_{3/2}3d^6_{5/2}4d_{3/2}$	6	2 884 760.6
				57	$3d^4_{3/2}3d^5_{5/2}4s^2$	6	3 856 300.0

TABLE V. Excitation-autoionization rates (in $sec^{-1}\,cm^3$) from the ground state of Zn-like Mo to the Cu ground state ($k=15$, see Table IV). Collisional excitation rate Q_{gj}, autoionization rate A_{jk}, decay rate, $\sum_l(A_{jl}+R_{jl})$, of the intermediate level j, and $X(g,j,k)$, the contribution of the level j to the total indirect ionization (via excitation-autoionization) rate $X(g,k)$. The number in square brackets is power of 10 factor.

			$T=100$ eV		$T=150$ eV	
j	A_{jk} (sec^{-1})	Decay rate	Q_{gj}	$X(g,j,k)$ ($sec^{-1}\,cm^3$)	Q_{gj}	$X(g,j,k)$
16	0.126[+14]	0.127[+14]	0.341[−11]	0.339[−11]	0.654[−11]	0.651[−11]
17	0.207[+14]	0.208[+14]	0.464[−11]	0.463[−11]	0.868[−11]	0.866[−11]
18	0.138[+12]	0.204[+12]	0.281[−11]	0.190[−11]	0.532[−11]	0.360[−11]
19	0.164[+12]	0.221[+12]	0.174[−11]	0.129[−11]	0.329[−11]	0.244[−11]
20	0.184[+13]	0.190[+13]	0.290[−11]	0.280[−11]	0.546[−11]	0.527[−11]
21	0.581[+13]	0.587[+13]	0.220[−11]	0.218[−11]	0.414[−11]	0.410[−11]
22	0.149[+12]	0.210[+12]	0.727[−11]	0.515[−11]	0.158[−10]	0.112[−10]
23	0.109[+13]	0.115[+13]	0.241[−11]	0.229[−11]	0.454[−11]	0.431[−11]
24	0.484[+13]	0.491[+13]	0.137[−09]	0.135[−09]	0.286[−09]	0.282[−09]
25	0.485[+12]	0.545[+12]	0.322[−11]	0.287[−11]	0.621[−11]	0.554[−11]
26	0.125[+14]	0.126[+14]	0.289[−11]	0.287[−11]	0.547[−11]	0.544[−11]
27	0.382[+12]	0.445[+12]	0.178[−11]	0.153[−11]	0.342[−11]	0.294[−11]
28	0.702[+13]	0.708[+13]	0.340[−11]	0.337[−11]	0.653[−11]	0.648[−11]
29	0.195[+12]	0.255[+12]	0.248[−11]	0.190[−11]	0.476[−11]	0.365[−11]
30	0.523[+11]	0.120[+12]	0.282[−11]	0.123[−11]	0.583[−11]	0.255[−11]
31	0.177[+12]	0.237[+12]	0.234[−11[	0.175[−11]	0.447[−11]	0.335[−11]
32	0.137[+16]	0.137[+16]	0.274[−11]	0.274[−11]	0.611[−11]	0.611[−11]
35	0.536[+12]	0.597[+12]	0.777[−12]	0.697[−12]	0.169[−11]	0.152[−11]
36	0.801[+12]	0.877[+12]	0.110[−10]	0.100[−10]	0.282[−10]	0.258[−10]

TABLE V. (*Continued*).

j	A_{jk} (sec^{-1})	Decay rate	$T=100$ eV Q_{gj} ($sec^{-1}\,cm^3$)	$T=100$ eV $X(g,j,k)$	$T=150$ eV Q_{gj}	$T=150$ eV $X(g,j,k)$
37	0.342[+12]	0.403[+12]	0.166[−11]	0.141[−11]	0.357[−11]	0.304[−11]
38	0.122[+14]	0.122[+14]	0.236[−11]	0.235[−11]	0.506[−11]	0.504[−11]
39	0.788[+13]	0.795[+13]	0.133[−11]	0.132[−11]	0.293[−11]	0.291[−11]
40	0.159[+12]	0.219[+12]	0.123[−11]	0.890[−12]	0.263[−11]	0.190[−11]
41	0.179[+12]	0.240[+12]	0.174[−11]	0.130[−11]	0.381[−11]	0.248[−11]
42	0.367[+13]	0.426[+12]	0.181[−11]	0.156[−11]	0.390[−11]	0.335[−11]
43	0.361[+13]	0.367[+13]	0.863[−12]	0.849[−12]	0.184[−11]	0.181[−11]
44	0.150[+13]	0.156[+13]	0.103[−11]	0.991[−12]	0.219[−11]	0.211[−11]
45	0.436[+12]	0.496[+12]	0.228[−11]	0.200[−11]	0.576[−11]	0.506[−11]
46	0.568[+13]	0.600[+13]	0.865[−10]	0.818[−10]	0.230[−09]	0.218[−09]
47	0.168[+12]	0.227[+12]	0.321[−11]	0.236[−11]	0.705[−11]	0.519[−11]
48	0.815[+13]	0.821[+13]	0.155[−11]	0.154[−11]	0.335[−11]	0.332[−11]
49	0.504[+13]	0.510[+13]	0.145[−11]	0.143[−11]	0.320[−11]	0.316[−11]
50	0.326[+12]	0.387[+12]	0.117[−11]	0.985[−12]	0.254[−11]	0.214[−11]
51	0.331[+12]	0.391[+12]	0.160[−11]	0.136[−11]	0.353[−11]	0.299[−11]
52	0.986[+11]	0.158[+12]	0.122[−11]	0.759[−12]	0.264[−11]	0.164[−11]
53	0.230[+12]	0.292[+12]	0.121[−11]	0.956[−12]	0.292[−11]	0.231[−11]
54	0.108[+15]	0.113[+15]	0.116[−11]	0.110[−11]	0.260[−11]	0.247[−11]
Total rates (in $sec^{-1}\,cm^3$)						
Indirect ionization $X(g,k)$				0.293[−09]		0.660[−09]
Direct ionization (Lotz)				0.465[−10]		0.153[−09]

j	$T=200$ eV Q_{gj}	$T=200$ eV $X(g,j,k)$	$T=275$ eV Q_{gi} ($sec^{-1}\,cm^3$)	$T=275$ eV $X(g,j,k)$	$T=350$ eV Q_{gj}	$T=350$ eV $X(g,j,k)$
16	0.846[−11]	0.842[−11]	0.976[−11]	0.971[−11]	0.101[−10]	0.100[−10]
17	0.110[−10]	0.110[−10]	0.122[−10]	0.122[−10]	0.122[−10]	0.122[−10]
18	0.676[−11]	0.457[−11]	0.759[−11]	0.513[−11]	0.762[−11]	0.515[−11]
19	0.419[−11]	0.310[−11]	0.469[−11]	0.347[−11]	0.469[−11]	0.347[−11]
20	0.692[−11]	0.668[−11]	0.772[−11]	0.746[−11]	0.771[−11]	0.745[−11]
21	0.524[−11]	0.519[−11]	0.583[−11]	0.577[−11]	0.581[−11]	0.575[−11]
22	0.227[−10]	0.161[−10]	0.299[−10]	0.212[−10]	0.343[−10]	0.243[−10]
23	0.576[−11]	0.546[−11]	0.643[−11]	0.610[−11]	0.643[−11]	0.610[−11]
24	0.397[−09]	0.392[−09]	0.498[−09]	0.491[−09]	0.551[−09]	0.544[−09]
25	0.799[−11]	0.712[−11]	0.907[−11]	0.808[−11]	0.917[−11]	0.817[−11]
26	0.694[−11]	0.690[−11]	0.775[−11]	0.771[−11]	0.775[−11]	0.771[−11]
27	0.438[−11]	0.377[−11]	0.493[−11]	0.424[−11]	0.496[−11]	0.426[−11]
28	0.843[−11]	0.836[−11]	0.964[−11]	0.956[−11]	0.986[−11]	0.978[−11]
29	0.609[−11]	0.466[−11]	0.687[−11]	0.526[−11]	0.690[−11]	0.528[−11]
30	0.802[−11]	0.350[−11]	0.999[−11]	0.436[−11]	0.110[−10]	0.480[−11]
31	0.571[−11]	0.428[−11]	0.640[−11]	0.479[−11]	0.641[−11]	0.480[−11]
32	0.872[−11]	0.872[−11]	0.112[−10]	0.112[−10]	0.125[−10]	0.125[−10]
35	0.228[−11]	0.204[−11]	0.268[−11]	0.240[−11]	0.275[−11]	0.247[−11]
36	0.443[−10]	0.405[−10]	0.633[−10]	0.578[−10]	0.771[−10]	0.704[−10]
37	0.480[−11]	0.408[−11]	0.559[−11]	0.475[−11]	0.568[−11]	0.483[−11]
38	0.679[−11]	0.676[−11]	0.788[−11]	0.784[−11]	0.800[−11]	0.796[−11]
39	0.405[−11]	0.402[−11]	0.492[−11]	0.488[−11]	0.524[−11]	0.520[−11]
40	0.354[−11]	0.256[−11]	0.410[−11]	0.297[−11]	0.416[−11]	0.301[−11]
41	0.521[−11]	0.388[−11]	0.621[−11]	0.463[−11]	0.647[−11]	0.482[−11]
42	0.525[−11]	0.451[−11]	0.610[−11]	0.525[−11]	0.620[−11]	0.533[−11]
43	0.244[−11]	0.240[−11]	0.281[−11]	0.276[−11]	0.283[−11]	0.278[−11]
44	0.293[−11]	0.282[−11]	0.338[−11]	0.325[−11]	0.343[−11]	0.330[−11]
45	0.891[−11]	0.783[−11]	0.124[−10]	0.109[−10]	0.147[−10]	0.129[−10]
46	0.370[−09]	0.350[−09]	0.543[−09]	0.514[−09]	0.674[−09]	0.637[−09]
47	0.962[−11]	0.709[−11]	0.113[−10]	0.832[−11]	0.117[−10]	0.862[−11]
48	0.453[−11]	0.450[−11]	0.528[−11]	0.524[−11]	0.538[−11]	0.534[−11]
49	0.439[−11]	0.434[−11]	0.526[−11]	0.520[−11]	0.551[−11]	0.545[−11]

TABLE V. (*Continued*).

j	$T=200$ eV Q_{gj}	$T=200$ eV $X(g,j,k)$	$T=275$ eV Q_{gj}	$T=275$ eV $X(g,j,k)$	$T=350$ eV Q_{gj}	$T=350$ eV $X(g,j,k)$
			($\sec^{-1}\,\mathrm{cm}^3$)			
50	0.343[−11]	0.289[−11]	0.400[−11]	0.337[−11]	0.408[−11]	0.344[−11]
51	0.484[−11]	0.410[−11]	0.578[−11]	0.490[−11]	0.602[−11]	0.510[−11]
52	0.356[−11]	0.222[−11]	0.414[−11]	0.258[−11]	0.421[−11]	0.262[−11]
53	0.433[−11]	0.342[−11]	0.575[−11]	0.454[−11]	0.657[−11]	0.519[−11]
54	0.359[−11]	0.342[−11]	0.429[−11]	0.408[−11]	0.444[−11]	0.422[−11]
Total rates (in $\sec^{-1}\,\mathrm{cm}^3$):						
Indirect ionization $X(g,k)$	0.963[−09]			0.128[−08]		0.148[−08]
Direct ionization (Lotz)	0.296[−09]			0.536[−09]		0.741[−09]

where

$$\phi^t(\mathbf{j}_a\mathbf{j}_b,\mathbf{j}_{a'}\mathbf{j}_{b'})=s_1X^t(\mathbf{j}_a\mathbf{j}_b,\mathbf{j}_{a'}\mathbf{j}_{b'})+s_2\sum_k(-1)^{k+t}[t]\begin{Bmatrix}j_a & j_{a'} & t\\ j_b & j_{b'} & k\end{Bmatrix}X^k(\mathbf{j}_a\mathbf{j}_b,\mathbf{j}_{b'}\mathbf{j}_{a'}) \tag{A2}$$

with $[t]\equiv 2t+1$, includes both direct and exchange Slater integrals (multiplied by the reduced matrices of the corresponding spherical harmonics):

$$X^t(\mathbf{j}_a\mathbf{j}_b,\mathbf{j}_{a'}\mathbf{j}_{b'})=(a\|c^{(t)}\|a')(b\|c^{(t)}\|b')R^t(\mathbf{j}_a\mathbf{j}_b,\mathbf{j}_{a'}\mathbf{j}_{b'}) \tag{A3}$$

and $s_1=1-\frac{1}{2}\delta_{aa'}\delta_{bb'}$, $s_2=(1-\delta_{ab})(1-\delta_{a'b'})$.

In Eq. (A1), i and j are electrons indices and a,b,a',b' represent sets of individual quantum numbers $\mathbf{j}_a\equiv n_al_aj_a$, etc. The dot in Eq. (A1) stands for scalar product and $\mathbf{Z}_i^{(t)}(\mathbf{j}_a,\mathbf{j}_{a'})$ are tensor operators of rank t defined by their reduced matrix elements

$$\langle\,\mathbf{j}_a\|\mathbf{Z}^{(t)}(\mathbf{j},\mathbf{j}')\|\mathbf{j}_b\,\rangle\equiv\delta_{\mathbf{j}\mathbf{j}_a}\delta_{\mathbf{j}'\mathbf{j}_b} \tag{A4}$$

with no parity restriction on the rank t.

APPENDIX B: THE DECOUPLING OF THE CONTINUUM FROM THE BOUND SYSTEM FOR AUTOIONIZATION

Substitution of Eq. (A2) in Eq. (5) yields

$$\mathsf{A}_{\psi}^{\psi''}=\sum_{\tilde{\mathbf{j}}}\sum_{J_T,M_T}\left|\left\langle\psi(\Gamma,J)\tilde{\mathbf{j}}J_TM_T\left|\sum_{\substack{i<j\\ i,j}}(e/r_{ij})\right|\psi''(\Gamma'',J_T'',M_T'')\right\rangle\right|^2$$

$$=\sum_{\tilde{\mathbf{j}}}\left[\sum_t\sum_{\mathbf{j}_0,\mathbf{j}_a,\mathbf{j}_b}\langle\psi\|(Z^{(t)}(\mathbf{j}_0,\mathbf{j}_a)\cdot\mathbf{Z}^{(t)}(\tilde{\mathbf{j}},j_b))\|\psi''\rangle\phi^t(\mathbf{j}_0\tilde{\mathbf{j}}\mathbf{j}_a\mathbf{j}_b)\right]. \tag{B1}$$

From the relations [2,17,18]

$$(\mathbf{Z}^{(t)}(\mathbf{j}_0,\mathbf{j}_a)\cdot\mathbf{Z}^{(t)}(\tilde{\mathbf{j}},\mathbf{j}_b))=(-1)^t(2t+1)[\mathbf{Z}^{(t)}(\mathbf{j}_0,\mathbf{j}_a)\times Z^{(t)}(\tilde{\mathbf{j}},\mathbf{j}_b)]^{(0)}\,, \tag{B2}$$

$$\mathbf{Z}^{(t)}(\tilde{\mathbf{j}},\mathbf{j}_b)=-(2t+1)^{-1/2}[\mathbf{a}_{\tilde{\mathbf{j}}}^{\dagger}\times\mathbf{a}_{\mathbf{j}_b}]^{(t)}=(-1)^{j+j_b-t}(2t+1)^{-1/2}[\mathbf{a}_{\mathbf{j}_b}\times\mathbf{a}_{\tilde{\mathbf{j}}}^{\dagger}]^{(t)}\,, \tag{B3}$$

where $\mathbf{a}_{\tilde{\mathbf{j}}}{}^{\dagger}$ and $\mathbf{a}_{\mathbf{j}_b}$, the creation and annihilation tensor operators are coupled to rank t, and the recoupling coefficient [17]

$$(t,(\mathbf{j}_b\mathbf{j})t|(t\,\mathbf{j}_b)\mathbf{j},\mathbf{j})^{(0)}=1 \tag{B4}$$

we can write

$$(\mathbf{Z}^{(t)}(\mathbf{j}_0,\mathbf{j}_a)\cdot\mathbf{Z}^{(t)}(\tilde{\mathbf{j}},\mathbf{j}_b))=(-1)^{\tilde{j}+j_b}[[\mathbf{Z}^{(t)}(\mathbf{j}_0,\mathbf{j}_a)\times\mathbf{a}_{\mathbf{j}_b}]^{(j)}\times\mathbf{a}_{\tilde{\mathbf{j}}}^{\dagger}]^{(0)}\,. \tag{B5}$$

Substitution of (B5) in (B1) and using Eqs. (3)–(35) of Ref. [17] together with the relation [18]

$$\langle\tilde{\mathbf{j}}\|\mathbf{a}_{\tilde{\mathbf{j}}}^{\dagger}\|0\rangle=-(2\tilde{j}+1)^{1/2}$$

we obtain

$$A_{\psi}^{\psi''}=\sum_{\tilde{j}}\left[\sum_{t}\sum_{j_0,j_a,j_b}(-1)^{J-J_T''+j_b}\langle\psi\|[\mathbf{Z}^{(t)}(\mathbf{j}_0,\mathbf{j}_a)\times\mathbf{a}_{j_b}]^{(\tilde{j})}\|\psi''\rangle\phi^t(\mathbf{j}_0\tilde{\mathbf{j}},\mathbf{j}_a\mathbf{j}_b)\right]^2 . \tag{B6}$$

Although the continuum was decoupled from the bound wave functions, the factorization in Eq. (B6) is incomplete since the operator still depends on the continuum through the rank j. However the values of this rank are restricted by triangular relation involving only bound orbitals and only few partial waves contribute.

The calculation of the bound angular matrix element is easily calculated by Eqs. (3)–(39) of Ref. [17],

$$\langle\psi\|[\mathbf{Z}^{(t)}(\mathbf{j}_0,\mathbf{j}_a)\times\mathbf{a}_{j_b}]^{(\tilde{j})}\|\psi''\rangle=\sum_{\psi'''}\begin{Bmatrix} j_b & \tilde{\mathbf{j}} & t \\ J & J''' & J'' \end{Bmatrix}\langle\psi\|\mathbf{Z}^{(t)}(\mathbf{j}_0,\mathbf{j}_a)\|\psi'''\rangle\langle\psi'''\|\mathbf{a}_{j_b}\|\psi''\rangle \tag{B7}$$

with the aid of the recoupling routine NJGRAF [19] and the relation [18]

$$\langle\mathbf{j}^{n-1}(\gamma_1 j_1)\|\mathbf{a}_{\mathbf{j}}\|\mathbf{j}^n(\gamma_2 j_2)\rangle=(-1)^n[n(2j+1)^{1/2}(j^{n-1}(\gamma_1 j_1)|\,\}j^n(\gamma_2 j_2)] , \tag{B8}$$

where $(j^{n-1}(\gamma_1 j_1)|\,\}j^n(\gamma_2 j_2)$ is the fractional percentages coefficient of equivalent orbitals $\mathbf{j}$.

---

*Permanent address: The Nuclear Research Center of the Negev, P.O. Box 9001, Beer-Sheva, Israel.

[1] M. S. Pindzola and S. L. Carter, Phys. Rev. A **22**, 898 (1980); Y. K. Kim and J. P. Desclaux, Phys. Scr. **36**, 796 (1987); P. L. Haglestein and R. K. Jung, At. Data Nucl. Data Tables **37**, 121 (1987).

[2] A. Bar-Shalom, M. Klapisch, and J. Oreg, Phys. Rev. A **38**, 1773 (1988).

[3] RELAC is the relativistic atomic structure code developed by M. Klapisch, A. Bar-Shalom, and E. Luc-Koenig. It is based on the parametric potential method [M. Klapisch, Comput. Phys. Commun. **2**, 239 (1971)]. This code calculates also radiative transition and probabilities.

[4] Hong Lin Zhang, Douglas H. Sampson, and Ajaya K. Mohanty, Phys. Rev. A **40**, 616 (1989).

[5] Hong Lin Zhang and Douglas H. Sampson, At. Data Nucl. Data Tables **43**, 1 (1989), and references therein.

[6] W. H. Goldstein, J. Oreg, A. Zigler, A. Bar-Shalom, and M. Klapisch, Phys. Rev. A **38**, 1797 (1988); W. H. Goldstein and R. S. Walling, *ibid.* **36**, 3482 (1987); W. H. Goldstein, B. L. Whitten, A. U. Hazi, and M. H. Chen, *ibid.* **36**, 3607 (1987); W. H. Goldstein, R. S. Walling, J. Bailey, M. H. Chen, R. Fortner, M. Klapisch, C. T. Phillip, and R. E. Stewart, Phys. Rev. Lett. **58**, 2300 (1987); M. Fikental, B. C. Stratton, H. W. Moos, A. Bar-Shalom, and M. Klapisch, Phys. Lett. **108A**, 71 (1985); J. F. Wyart, C. Bauche-Arnoult, J. C. Gauthier, J. P. Geindre, P. Monier, M. Klapisch, A. Bar-Shalom, and A. Cohn, Phys. Rev. A **34**, 701 (1986).

[7] M. H. Chen and B. Crassemann, Phys. Rev. A **10**, 2232 (1974).

[8] P. Mandelbaum, M. Finkenthal, E. Meroz, J. L. Schwob, J. Oreg. A. Bar-Shalom, W. H. Goldstein, M. Klapisch, S. Lippman, L. K. Huang, and H. W. Moos, Phys. Rev. A **42**, 4412 (1990).

[9] M. Finkental, S. Lippman, L. K. Huang, T. L. Yu, B. C. Stratton, H. W. Moos, M. Klapisch, P. Mandelbaum, A. Bar-Shalom, W. L. Hodge, P. E. Phillips, T. R. Price, J. C. Porter, B. Richards, and W. L. Rowan, J. Appl. Phys. **59**, 3644 (1986).

[10] W. L. Hodge, M. Finkental, H. W. Moos, S. Lippman, L. K. Huang, A. Bar-Shalom, and M. Klapisch, Rev. Sci. Instrum. **55**, 16 (1984).

[11] W. H. Goldstein, A. Osterheld, J. Oreg, and A. Bar-Shalom, Astrophys. J. **344**, L37 (1989).

[12] R. D. Cowan, *The Theory of Atomic Structure and Spectra* (University of California Press, Berkeley, 1981).

[13] M. H. Chen (private communication).

[14] I. I. Sobelman, L. A. Vainshtein, and E. A. Yukov, *Excitation of Atoms and Broadening of Spectral Lines* (Springer-Verlag, Berlin, 1981).

[15] J. Oreg, Ph.D. thesis, The Hebrew University, Jerusalem, 1973.

[16] J. Oreg, W. H. Goldstein, A. Bar-Shalom, and M. Klapisch, Phys. Rev. A **39**, 4599 (1989).

[17] B. R. Judd, *Operator Techniques in Atomic Spectroscopy* (McGraw-Hill, New York, 1963).

[18] B. R. Judd, *Second Quantization and Atomic Spectroscopy* (Johns Hopkins Press, Baltimore, 1967).

[19] A. Bar-Shalom and M. Klapisch, Comput. Phys. Commun. **50**, 375 (1988).